# POLSA sensor network capabilities under different operating modes

**Tomasz Zubowicz**[*,1], **Mikołaj Krużyński** [1], **Krzysztof Armiński** [1], **Mikołaj Karawacki** [1], **Krzysztof Szyszka** [1], **Marcin Teofilewicz** [2], **Artur Makarewicz** [2], **Edwin Wnuk** [1], **Zygmunt Anioł** [2], **Tymoteusz Trocki** [2]

[1] *Dept. of Space Safety, Polish Space Agency, Trzy Lipy 3 Street,* 80-172 *Gdańsk, Poland*

[2] *Dept. of Space Safety, Polish Space Agency, Prosta* 70 *Street,* 00-838 *Warszawa , Poland*

**Abstract**

This paper demonstrates the capabilities of the POLSA Observational sensor Network (POLON) developed by the Polish Space Agency (POLSA). The POLON includes five locations, Australia, South Africa, Chile, the newly developed continental United States and Hawaii, consisting of a total of twenty configurations. The sensor at each location can operate as a single grid-based sensor or a group of individual instruments. The sensors consist of telescopes with an aperture of approximately thirty centimeters (approximately 11.81 in) on high-speed mounts capable of tracking even the fastest satellite objects and are equipped with state-of-the-art CMOS cameras. The study primarily compared sensor performance and observation efficiency using well-defined metrics, including the number of (unique) objects observed and tracks generated, (average) observation arc length, revisit time, and accuracy interpreted in terms of root mean square (RMS) error, in survey and tracking modes. The observational data required for these analyses were collected during several observation campaigns. Observations have been carried out for space objects in LEO, MEO, and GEO regimes. The results of this study provide a concise description of the POLON architecture and illustrate its performance and efficiency in observing space objects.

## 1. INTRODUCTION

Challenges related to space operations safety, asset sustainability and security in the space domain continue to grow, driven by scientific, technological, commercial and geopolitical changes. To face these challenges, one needs to take action, which cannot be done without having an understanding and knowledge of the environment within which they arise. This is one of a fundamental driving factors for the development and advancement of the existing space surveillance sensor networks and associated (software) information and knowledge extraction mechanisms. These activities add tangible and justified value to the services and are an important initial step toward enhanced space surveillance and tracking (SST) and space situational awareness (SSA).

Modern SSA systems are inherently heterogeneous, characterized by diversity and complexity at multiple levels. From an administrative and organizational perspective, these systems fall under the management of civilian or military organizations, reflecting their dual use in ensuring both civilian spaceflight safety and national security. Data-sources for SSA are equally diverse. These include contributions from a wide range of sensors that include ground-based telescopes, radars, and (laser, optical or radio frequency) ranging stations, as well as space-based optical systems or radio frequency monitoring instruments. This plethora of sensors generates data that spans a variety of wavelengths and modalities, requiring high-end information exchange structures and multi-spectrum algorithms and applications to efficiently process and analyze the information. Thus the algorithms used for SSA are tailored to integrate and interpret this heterogeneous data, offering comprehensive insights into the behavior of space objects, orbital debris and potential threats. Such a design enables SSA systems to fulfill the critical role they play in preserving space security while maintaining adequate operational efficiency.

Also, it is the case for the SST component which depends on the availability of data from measurements and observations of artificial Earth satellites. These are crucial to the operations and evolution of SST systems. Data fusion from a variety of sources increases the synergistic use of the available information [1], which translates to a reduction in the uncertainty associated with the knowledge of the state and operational conditions of the object of interest [2].

Poland has an extensive experience in optical and laser observations of artificial satellites and space debris, as well as in orbital dynamics of those objects. First visual observations of artificial Earth's satellites, including Sputnik 1, were performed in

*Corresponding author, e-mail: tomasz.zubowicz@polsa.gov.pl

1957 in the Astronomical Observatory of Adam Mickiewicz University (AO AMU), Poznan. In the next years simple optical cameras were used for satellite observations in AO AMU, Warsaw University Astronomical Observatory and Borowiec Astrogeodynamic Observatory (BAO) being a part of the Space Research Centre of the Polish Academy of Sciences (SRC PAS). Professional optical astrometric observations of artificial satellites started in early 1960's and were continued up to late 1980's by AO AMU and at the BAO. These observations were performed with the use of dedicated optical telescopes designed and built by AO AMU, and later with the use of Carl Zeiss SBG camera purchased by BAO. The SRC PAS together with AO AMU developed satellite laser ranging station in BAO. The first generation laser began observing passive geodetic satellites in 1976, and the second generation laser ranging system, fully designed and developed in Poland [3], is performing observations since 1988 up to now, after several modernizations [4]. Since 2015 AO AMU carries out optical observations of artificial satellite objects, including space debris, using fully robotic 0.7 m telescope located in Sonoita, Arizona, USA [5].

When Poland joined the European EUSST consortium in 2018, three major optical sensor networks belonging to scientific institutions and commercial entities were in operation. Although not initially designed for SST observations, these sensors were adopted and used for such a purpose. First was the Global Astrophysical Telescope System (GATS) of AO AMU, which included 0.5 m and 0.7 m optical telescopes designated PST1 and PST2 and was located in Poland and Arizona, USA, respectively [6]. These two instruments, particularly PST2, provided high-accuracy astrometry even for LEO purposes [7]. Second was owned by the Nicolaus Copernicus Astronomical Center of the Polish Academy of Sciences, a network of three 0.5 m Solaris telescopes located in Australia, Argentina, and South Africa [8]. Third was a network owned by a private company named 6ROADS, consisting of six telescopes with diameters ranging from 0.14 m to 0.4 m, located in Poland, Sweden, Italy, Spain, and Chile [9].

In the following years, AO AMU developed a new sensor dedicated to optical observations of satellites and space debris, the Poznan SST 3 (PST3) telescope cluster. This instrument consists of five individual telescopes ranging in size from 0.3 m to 0.7 m and a field of view (FoV) of up to 3.2 deg $\times$ 2.7 deg and has been deployed at the Center for Nature Education in Chalin, Poland [10]. Also, the 6ROADS company expanded its network of optical telescopes dedicated to SST observations. Currently, in 2024, it comprises fourteen telescopes in eleven observatories located in Spain, Italy, Chile, Poland, Japan, USA, Namibia, and Australia.

The POLSA Observational sensor Network (POLON), operated by POLSA Operational Center (SSAC-PL), establishes a national SST capability for passive optical observations used to monitor objects in Earth's orbits and, in this role, is foreseen as a part of the draft of the National Space Program for 2021–2026. It provides the foundation for further development of a network of ground-based optical sensors in various technical and organizational configurations for SST observations. Also, the POLON is a part of the SSA component of the EU Space Program set up to establish a part of the European SST Partnership service provision function [11].

The contribution and operations of POLON include not only providing the necessary data, but also ensuring redundancy while taking into account economic factors. Redundancy is crucial in sensor networks to increase reliability and ensure uninterrupted operation despite the individual component failures [12]. Thus, the integrity of data collection and processing is maintained. The design of such networks requires a conscientiously optimized architecture that balances technical efficiency with economic considerations [13]. The design involves more than just structural aspects; it integrates data fusion techniques, real-time processing and economic efficiency [14, 15]. Pivotal in such a case is the issue of simultaneous design of the system and its algorithms, since their interactions can result in synergistic effects that substantially increase both the performance and reliability of the overall system [16]. Such a design approach ensures harmonious operation of hardware and software components, optimizing the overall functionality of the network [15] and provided services [17].

In the previous work, authors proposed an approach to the allocation of sensor network operating time at the stage of business objective planning with the inclusion of the performance and produced data quality criteria [15]. In this work the focus is set on operational activities — performance of individual POLON elements as well as on the cooperation of these elements as a system of systems. In the first case, the evaluation is carried out through the prism provided by statistical tools. In the second case, evaluation is carried out by assessing the quality metrics related to products generated by Polish Space Agency (POLSA) analytical engines based on POLON generated data. Here the authors use the orbit determination (OD) process to illustrate the POLON capabilities. In the frame of this article, several typical examples of such an operation have been shown. The rationale for this approach is as follows. Innovation plays a key role in transforming raw data into accurate state estimates through the use of advanced estimation and information theory methods and tools. Techniques such as batch optimization and filtering methods help reduce uncertainty and increase the precision of state estimates, which is critical to maintaining reliable SST operations. For example, the Kalman filter uses these principles to optimally combine noisy measurements and dynamic models, thereby improving the accuracy of state estimates [18]. These are considered essential for achieving real-time situational awareness.

The contribution of the article is as follows. A comparison was made between sensor performance and observation efficiency using well-defined indicators in different modes of operation, including survey and tracking. A feasibility study of POLON survey and tracking scheduling and system level response has been documented for geostationary orbit (GEO), medium Earth orbit (MEO), and low Earth orbit (LEO) regimes. An astrometric and orbital analysis based performance of the POLON-based data has been indicated. A case-based illustration of the POLON capabilities is provided.

The reminder of this paper is organized in the following manner. A problem formulation has been provided in Section 2. Sections 3 and 4 provide technical description of POLON and sensor site configuration. Section 5 documents the conducted experiments. Finally, Section 6 concludes the paper.

## 2. PROBLEM FORMULATION

Let a SST system ($\Omega_{\mathrm{SST}}$) be taken under consideration. In general terms, it is assumed to consist of a sensory network ($\Omega_{\mathrm{WSN}}$), one or many, and a system that provides the data warehousing capabilities to facilitate data and information processing and report and (analytical) product generation and conveying ($\Omega_{\mathrm{DW}}$). The system in such a configuration is used to assess the state and operational conditions in a certain neighborhood of the Earth. Moreover, typical architectural features of such a system include a number of weak and strong interconnections with other external information services of vital importance to its operation. The problem addressed in this paper focuses on evaluating the performance of the sensory network subsystem ($\Omega_{\mathrm{WSN}}$) using the POLON network as an example. The evaluation process is carried out based on the data provided by this network ($\Omega_{\mathrm{M}}$) to POLSA systems by means of the statistical tools with regard both to the POLON data itself and the products ($\Omega_{\mathrm{P}}$) generated by the analytical subsystem ($\Omega_{\mathrm{AE}}$) of the POLSA data warehouse ($\Omega_{\mathrm{DW}}$). The described configuration of the SST system is illustrated in Fig. 1.

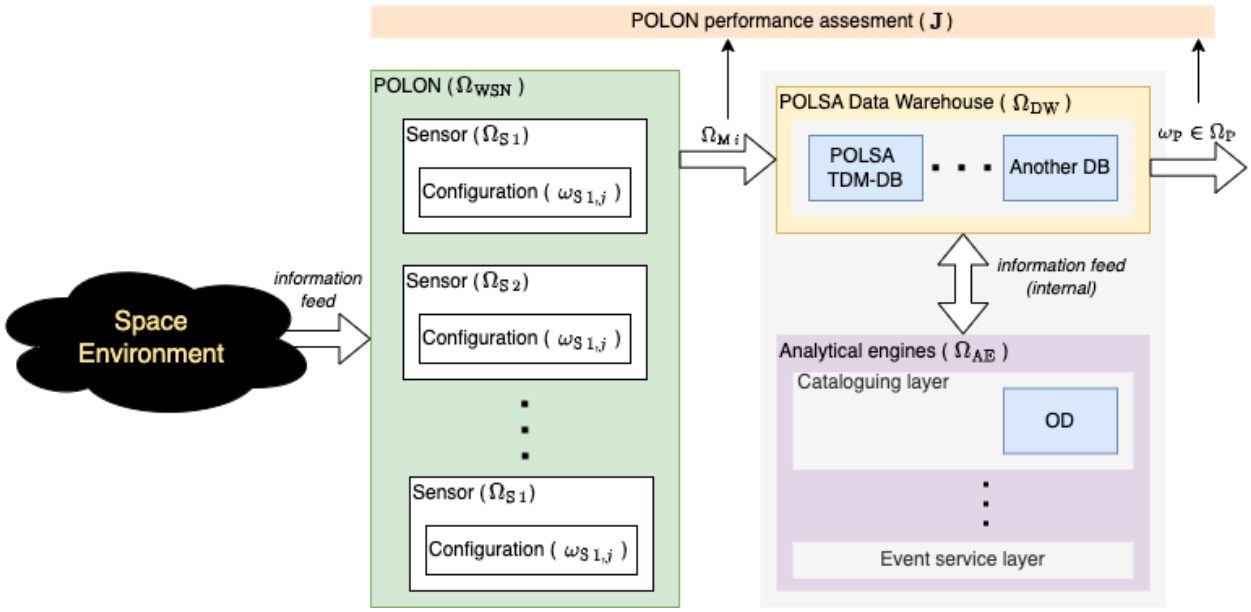


Figure 1: Space surveillance and tracking system configuration

Formally, the problem is described as follows. Let $\mathbb{N}$ denote the natural numbers. Then by taking $\omega_{\mathrm{Si,j}} \in \Omega_{\mathrm{Si}}$ to denote $j$th individual passive optical sensor (telescope) as a sensor configuration, $j \in \overline{1, n_{Ci}} \subset \mathbb{N}$, located at $\Omega_{\mathrm{Si}}$ (sensor) site of all $n_{\mathrm{S}} \in \mathbb{N}$ sites considered, with $i \in \overline{1, n_{\mathrm{S}}} \subset \mathbb{N}$, the $\Omega_{\mathrm{WSN}} \stackrel{\mathrm{def}}{=} \bigcup_{i \in \overline{1,n_{\mathrm{S}}}} \Omega_{\mathrm{Si}}$ spans the POLON worldwide sensor network (WSN). Each sensor site, $\Omega_{\mathrm{Si}}$, $\forall i$, generates (standardized) observation based data packets $\Omega_{\mathrm{Mi}}$ that are conveyed to POLSA data warehouse $\Omega_{\mathrm{DW}}$ for analytical product generation and reporting ($\omega_{\mathrm{P}} \in \Omega_{\mathrm{P}}$). The performance of the SST system is then assessed based on the $\Omega_{\mathrm{Mi}}$ and $\omega_{\mathrm{P}}$ using a collection of metrics, $\boldsymbol{J} \stackrel{\mathrm{def}}{=} \left[\boldsymbol{J}_{\mathrm{M}}^{T}, \boldsymbol{J}_{\mathrm{P}}^{T}\right]^{T}$, as defined in the following lines.

The evaluation of the observational data generated by the sensors and their configurations shall be assessed based on the evaluation criteria $\boldsymbol{J}_{\mathrm{M}} \stackrel{\mathrm{def}}{=} [J_{\mathrm{MMEAS}}, J_{\mathrm{MSO}}, J_{\mathrm{MUSO}}, J_{\mathrm{MARMS}}, J_{\mathrm{MLARC}}]^{T}$, where: $J_{\mathrm{MMEAS}}$ is the number of measurements per data-set, $J_{\mathrm{MSO}}$ denotes total number of space objects observed, $J_{\mathrm{MSO}}$ it the total number of unique space objects observed, $J_{\mathrm{MARMS}}$ is the astrometric root mean square (RMS), $J_{\mathrm{MLARC}}$ signifies observed arc length of each $\Omega_{\mathrm{Mi}}$,

The evaluation of the accuracy of the generated products ($\omega_{\mathrm{P}}$) has been carried out based on the RMS of OD in right ascension ($J_{\mathrm{PRA}}$) and declination ($J_{\mathrm{PDEC}}$), thus $\boldsymbol{J}_{\mathrm{P}} \stackrel{\mathrm{def}}{=} [J_{\mathrm{PRA}}, J_{\mathrm{PDEC}}]^T$.

The experiments and analyses conducted were limited by the following assumptions.

**Assumption 1** *POLON sensors operate under daily-basis operational conditions.*

The Assumption 1 implies that each sensor ($\omega_{\mathrm{S}}$) state or condition is operational, functional, and ready for its intended purpose during period of consideration. Also, this implies that each sensor or sensor site is subject to environmental disturbances, e.g., weather conditions, that influence its state and disrupts the operational capabilities.

## 3. POLON ARCHITECTURE

Given the assessment of feasible set of sensor locations, based on performance, maintenance, economic and weather conditions as well as the availability of existing support, the POLON sites include: Siding Spring Observatory in Australia (SSO), South African Astronomical Observatory in the Republic of South Africa (SAAO), DeepSkyChile in Chile (DSC), Utah Desert Remote Observatories (UDRO), and Moloka'i Observatory (MO). The POLON has been depicted in Fig. 2.

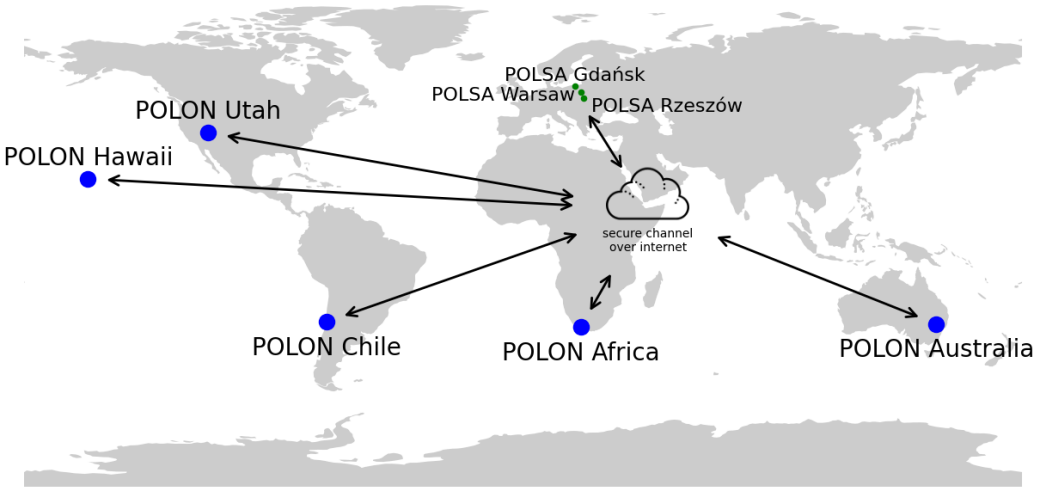


Figure 2: POLON geospatial localization

The corresponding coordinates have been collated in Table 1.

Table 1: Telescope sites locations

| No. ($i \in \overline{1, n_{\mathrm{s}}}$) | Site ($\Omega_{\mathrm{S}i}$) | Observatory | Location | | |
|---|---|---|---|---|---|
| | | | Longitude [deg] | Latitude [deg] | Altitude [m] |
| 1 | POLON-Australia | SSO | 149.06979 | −31.27344 | 1116 |
| 2 | POLON-Africa | SSAO | 20.80969 | −32.38004 | 1760 |
| 3 | POLON-Chile | DSC | −70.85309 | −30.52636 | 1708 |
| 4 | POLON-Utah | UDRO | −113.69735 | 37.73798 | 1575 |
| 5 | POLON-Hawaii | MO | −156.94110 | 21.07243 | 98 |

SSO - Siding Spring Observatory https://www.sidingspringobservatory.com.au/
SSAO - South African Astronomical Observatory https://www.saao.ac.za/
DSC - Deep Sky Chile https://www.deepskychile.com/
UDRO - Utah Desert Remote Observatories, USA https://utahdesertremote.com/
MO - Moloka'i Observatory, Hawaii, USA (no website)

The daily operation of POLON follows the paradigm illustrated in Fig. 1.

## 4. SENSOR SITE DESIGN

**Physical layer** In Fig. 3, a typical layout of a single location is depicted using POLON-Africa ($\Omega_{S2}$) as an example. Each site (($\Omega_{Si}$, $\forall i$)) consists of four ($n_{Ci} = 4$, $\forall i$) identical configurations ($\omega_{Si,j}$, $\forall i, j$). A single configuration ($\omega_{Si,j}$) comprises an ASA UWF300-type telescope (A) attached to a PlaneWave L-350 mount (B) in a horizontal configuration. The image from the telescope is acquired with a QHY411 camera (C) mounted in the primary focus (D). A dedicated industrial computer (E) controls each of the sets thus organized. Accurate time is provided by a GNSS clock (F) directly connected to the cameras and NTP server. The protective shelter for the infrastructure elements includes a pavilion with a sliding roof (G). The roof opening status is controlled automatically or manually and depends on the time of day and meteorological conditions monitored by a system using a weather station (H). The site is under continuous monitoring by a CCTV camera system (I).

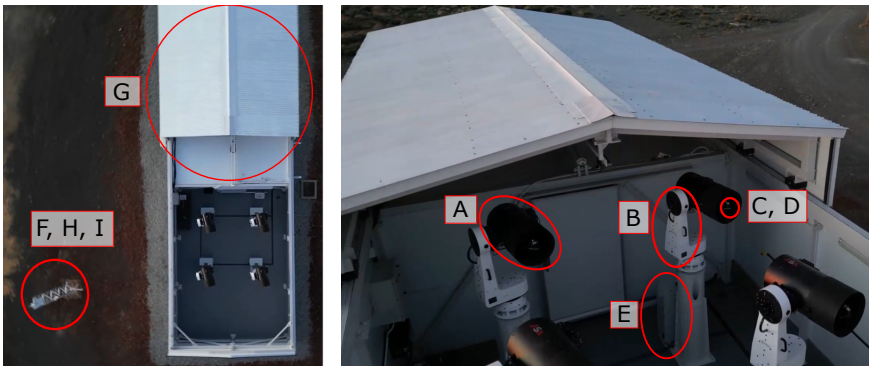


Figure 3: Example configuration: POLON-Africa ($\Omega_{S2}$)

Fundamental technical parameters of single configuration have been collated in Table 2.

Table 2: Technical parameters of a single configuration (telescope)

| Parameter | Unit | Value |
|---|---|---|
| Aperture | mm | 300.0 |
| Focal length | mm | 390 |
| Camera resolution | px × px | 14304 × 10748 |
| field of view (FoV) | deg × deg | 7.90 × 5.94 |
| Pixel scale | arcsec/px | 1.99 |
| Maximum frame rate | fps | 10 |
| Maximum mount speed | deg/s | 50 |

**Field control and monitoring** Each site is capable of operating in one of three control modes: remote control under operator supervision, in automatic mode or autonomously. In each case, this control actions are executed by suitably designed algorithms, which utilize the hardware drivers of the installed components for this purpose. These algorithms are executed in the physical layer incorporating dedicated and redundant industrial computers and servers, used to coordinate their operation. Process monitoring is performed in multiple layers. Starting from the hardware layer, through processing algorithms and network services, which allows operators to quickly respond to changing conditions and the operating state of the equipment, if necessary. Dedicated environments and communication protocols used for this purpose enable business analytics in POLSA's virtual operating environment ($\Omega_{DW}$, $\Omega_{AE}$).

**Sensor tasking** In most cases, sensor scheduling is handled using dedicated software tools, that, taking into account hardware and operational limitations, considerably support the operator's work. The observations can be conducted in tracking or survey mode. In the first case, the essential information required for the preparation of an observation task is a list of object identifiers admissible for observation (typically NORAD ID) including priorities and desired exposure times. In the second case, instead of object identifiers, coordinates implementing the survey strategy are provided. Also, the telescope's software allows observation of an arbitrary objects that do not have an identifier in the POLSA systems based on an orbit description

in the Two-line element set (TLE) format. Typically, a window of 15 min is allocated for a single observation task, known as an observation slot. The software allocates the desired targets to each slot, taking into account task parameters and priorities. If possible, the remaining time in the slots is allocated to optional targets to maximize the use of available observation time. At each stage, the operator has the flexibility to adjust the scheduling strategy and a targets considered to observation slots.

**Data acquisition, storage and processing** The image captured by the camera is stored in FITS format files. Each acquisition task is augmented with meta data related to the parameters characterizing the task. The prepared dataset is the input subject to processing.

Considering the very high volume of data generated and the limitations of communication bandwidth, POLON implements an edge processing paradigm - processing the data on-site. Image processing is done in a decentralized environment. Each configuration is responsible for processing the data it generates. A dedicated astrometry engine based on the astrometry24.NET service is used for this purpose. It combines data reduction and preliminary analysis, resulting in an intermediate product in the form of a JavaScript Object Notation (JSON) file [19]. Among other things, it contains information about: position and brightness of all extracted features, both in frame coordinates and sky coordinates, as well as rolling shutter corrections; correlation of features with stars and known catalog objects; translation between frame coordinates and sky coordinates, with RMS; Flexible Image Transport System (FITS) header information; time and location information; and other necessary presets for successful processing.

The intermediate product is then used to create CCSDS Tracking Data Message (TDM) ($\Omega_{\mathrm{M}}$). A single TDM file will contain only one tracklet for a single object. If multiple objects were observed and correlated in the previous step, more files will be created. In addition, a procedure called 'tracklet linking' is performed. Features that were not correlated, but have changed location in subsequent images in a consistent manner, are detected and used to create TDMs with temporary identification numbers. In rejection of false positive results due to, for example, cosmic rays or other artifacts, at least three points are required to form a TDMs.

Each location is equipped with a disk array for temporary data archiving, which is essential for system maintenance.

## 5. EXPERIMENTS

This section is divided into two parts. Subsection 5.1 presents the preparation of experiments, including the use of methods and tools. In turn, Subsection 5.2 provides an insight into the results obtained. Further, to highlight the usefulness of POLON, the results subsection has been supplemented with a section illustrating the contribution of this sensor network to the observations of high interest events that have occurred in Earth's orbits recently — see Subsection 5.2.4.

### 5.1 Setup

Taking into account the daily activities of POLON, five observation campaigns were planned for execution throughout June till early August. Each campaign period was planned *a priori* without taking into account factors other than those arising from business and organizational constraints. Thus, weather-related availability or scheduled maintenance activities became a business as usual (BAS)-type factor influencing operational efficiency. Each activity has been associated with either GEO, MEO or LEO regimes. In the case of the GEO campaign, scheduling in both survey and tracking modes was considered. The survey part was distributed over three independent time periods. In each case only three sites of the POLON did participate in the campaign, namely POLON-Africa, POLON-Australia, and POLON-Chile (Fig. 2 or Table 1). In Table 3 a summary characterizing these activities have been presented.

Table 3: Observational campaign characterization

| Campaign* | Part | Epoch (UTC) | | Participant/Site |
|---|---|---|---|---|
| | | Start | Stop | |
| GEO-S | 01 | 2024-06-12T00:00:00.000 | 2024-06-13T00:00:00.000 | POLON-Africa |
| | 02 | 2024-06-17T17:00:00.000 | 2024-06-20T20:00:00.000 | POLON-Australia |
| | 03 | 2024-07-05T17:30:00.000 | 2024-07-08T04:45:00.000 | POLON-Chile |
| GEO-T | | 2024-07-09T19:15:00.000 | 2024-07-23T12:00:00.000 | |
| LEO-T | | 2024-07-05T17:30:00.000 | 2024-07-08T04:45:00.000 | |

* (S)urvey, (T)racking.

To maintain control over the assets' performance and to determine the fundamental measurement models during the individual campaigns, MEO navigation objects from the GALILEO constellation and selected International Laser Ranging Service (ILRS) objects from the LEO regime were included in the daily observation schedules. The indicators for the periods of the individual campaigns, assessing the residual measurements in relation to the precise ephemerides, published for these objects in the form of Extended Standard Product 3 (SP3) format, in an average sense, have been investigated.

### 5.2 Results and discussion

The following subsections deal with the results obtained during the GEO-S, GEO-T, and LEO-T campaigns, respectively (see Subsection 5.1). Each subsection is organized as follows. First, the observational conditions at each location (Tables 1 and 3) have been presented. Second, statistics on sensor performance were presented. In the case of GEO-S and LEO-T campaigns, an OD based evaluation results have been provided.

#### 5.2.1 Experiment 1: GEO survey

**POLON operational conditions** By virtue of Assumption 1, the availability of sensor locations is presented based on conditions and operational status. Since the telescopes in each location share the same constraints (Section 4), only one timeline is presented. For practical reasons, weather changes on a long time scale of more than 5 minutes were included. Hence, taking into account all three stages of the GEO-S campaign, its total duration reached 4 days. During this period, given the observational conditions and the operational status of the assets, the observational opportunities available at each location have been illustrated in Fig. 4. The red dashed vertical lines indicate parts of the GEO-S campaign — see Table 3. Site POLON-Australia was accessible for about 1 d 19 h hours (53.5% of the theoretically available time[1]), POLON-Chile for 2 d (59.4% of the theoretically available time), and POLON-Africa for 16 h (17.2% of the theoretically available time). Most of the unavailability of the sensors during the period of the GEO-S was due to on-site weather conditions.

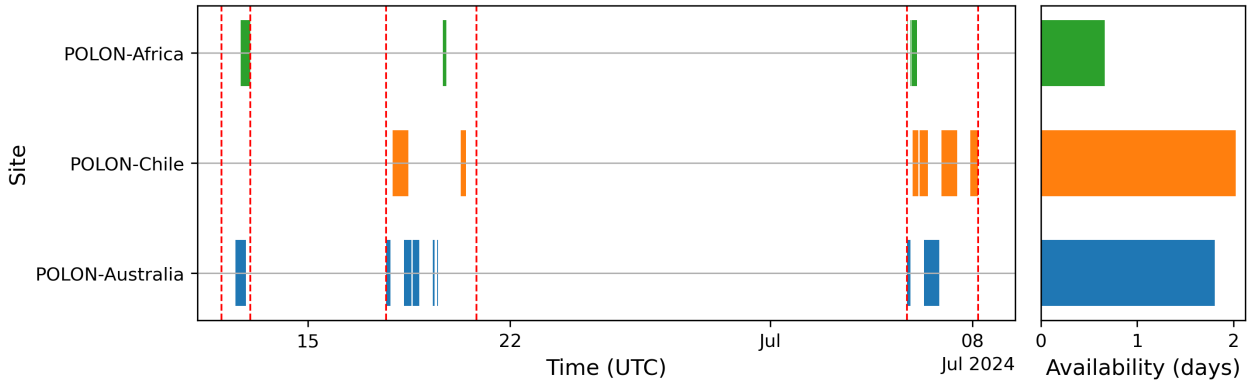


Figure 4: Availability of sensors for observations per site during GEO-S campaign

**POLON performance** The POLON system performance indicators for the GEO experiment have been summarized in Table 4. These indicators demonstrate a high overall throughput of POLON sensors. It follows from a comparison of the number of observed objects in relation to theoretically possible observations interpreted through the prism of the observation available time (Fig. 4). Also, referring to the number of observed *unique* objects, part 01 of the experiment resulted in the observation of 599 out of the theoretically estimated observable 1168 objects, with 324 of 1167 and 582 of 1531 for parts 02 and 03, respectively. Taking into consideration relatively bad weather during GEO-S, particularly noteworthy is part 02, which significantly deviates from the others, it follows that sensor performance was acceptable. Moreover, considering the type of campaign and data acquisition strategy used the maximum observable arc length of 3.75 deg has been recorded. Finally, it follows that such campaigns should essentially incorporate redundancy by doubling observational time.

[1] Cumulated time of civil night during the relevant period

Table 4: GEO-S campaign performance statistics

| Metric ($\boldsymbol{J}_{\mathrm{M}}$) | Unit/Format | Value min | max | median | mean | std | total |
|---|---|---|---|---|---|---|---|
| | | | | Part 01 | | | |
| Astrometric RMS ($J_{\mathrm{MARMS}}$) | arcsec | 0.13 | 0.73 | 0.28 | 0.29 | N/A | N/A |
| Arc Length ($J_{\mathrm{MLARC}}$) | deg | 0.00 | 3.22 | 0.78 | 0.84 | N/A | N/A |
| No. of measurements ($J_{\mathrm{MMEAS}}$)** | | 3 | 326 | 34 | 56 | 57 | 295135 |
| Objects observed ($J_{\mathrm{MSO}}$)* | | | | | | | 5296 |
| Unique objects ($J_{\mathrm{MUSO}}$) | | | | | | | 599 |
| Unique objects (theoretical) | | | | | | | 1168 |
| | | | | Part 02 | | | |
| Astrometric RMS ($J_{\mathrm{MARMS}}$) | arcsec | 0.14 | 1.96 | 0.28 | 0.26 | N/A | N/A |
| Arc Length ($J_{\mathrm{MLARC}}$) | deg | 0.01 | 2.57 | 0.61 | 0.79 | N/A | N/A |
| No. of measurements ($J_{\mathrm{MMEAS}}$)** | | 3 | 279 | 27 | 51 | 57 | 45318 |
| Objects observed ($J_{\mathrm{MSO}}$)* | | | | | | | 881 |
| Unique objects ($J_{\mathrm{MUSO}}$) | | | | | | | 324 |
| Unique objects (theoretical) | | | | | | | 1167 |
| | | | | Part 03 | | | |
| Astrometric RMS ($J_{\mathrm{MARMS}}$) | arcsec | 0.13 | 0.97 | 0.25 | 0.25 | N/A | N/A |
| Arc Length ($J_{\mathrm{MLARC}}$) | deg | 0.01 | 2.45 | 0.63 | 0.82 | N/A | N/A |
| No. of measurements ($J_{\mathrm{MMEAS}}$)** | | 3 | 292 | 37 | 67 | 67 | 150673 |
| Objects observed ($J_{\mathrm{MSO}}$)* | | | | | | | 2245 |
| Unique objects ($J_{\mathrm{MUSO}}$) | | | | | | | 582 |
| Unique objects (theoretical) | | | | | | | 1531 |

* No. of objects observed is equivalent to number of TDMs generated ($\Omega_{\mathrm{M}}$) — recall Section 4: Data acquisition, storage and processing.

** The statistics are given per TDM.

Revisit histograms[2] are presented in Fig. 6. Assuming that those of the GEO objects that do not perform substantial maneuvers do not require excessively frequent observation to maintain the orbit the results presented indicate that POLON was used effectively during the campaign, where most of the objects were observed once (no re-visits) during the course of the experiment.

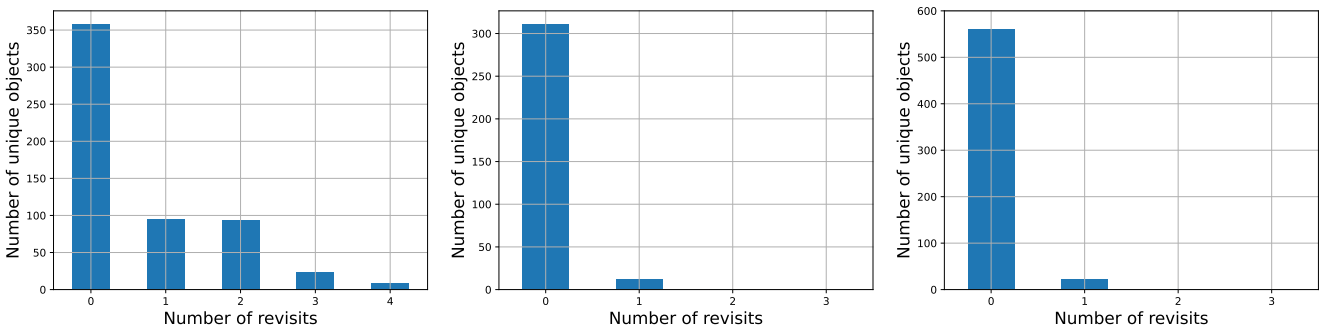


(a) Campaign part no. 1 (b) Campaign part no. 2 (c) Campaign part no. 3

Figure 6: POLON unique objects revisits during GEO-S campaign

**OD based assessment** The orbital accuracy of the observations acquired during the GEO survey campaign was assessed using the QZS constellation object, namely QZS-3 (MICHIBIKI-3). Object details have been provided in Table 5.

[2]GEO revisit is defined as an observation made during different nights or separated =observation slots.

Table 5: QZS-3 satellite object characterization

| Parameter | Unit/Format | Value | Source/Description |
|---|---|---|---|
| Object name | N/A | QZS-3 (MICHIBIKI-3) | space-track.org |
| NORAD ID | N/A | 42917 | space-track.org |
| COSPAR ID | N/A | 2017-048A | celestrak.org |
| Type | N/A | Payload | space-track.org |
| Avg. cross-section | $m^2$ | 35.9524 | discosweb.esoc.esa.int |
| Mass | kg | 4700.0 | discosweb.esoc.esa.int |
| Launch date | UTC | Aug 19, 2017 | space-track.org |

Due to orbital regime only POLON-Australia had observation access to the QZS-3 object. The observation acquisition events over the GEO-S campaign horizon have been illustrated and counted in Fig. 7.

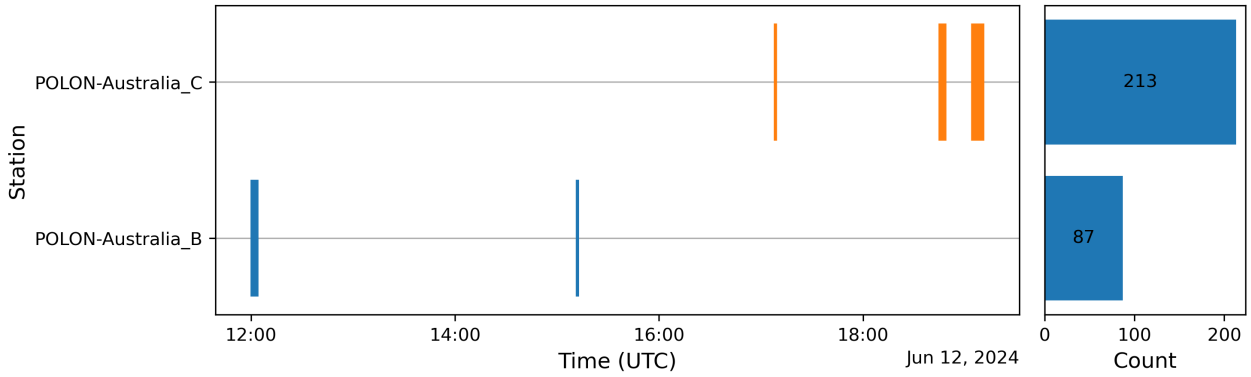


Figure 7: Observation events of satellite QZS-3 (NORAD ID: 42917)

In Fig. 8 a cutout from a photo, in FITS format, captured using exposure time of $2s$ and binning $2 \times 2$, during the GEO-S experiment, with POLON-Australia_B telescope on 17.06.2024 at $12:29:33$ UTC (mid-exposure) indicating the position of QZS-3 satellite (Table 5) has been presented. The original frame center coordinates yields: $\alpha = 14^{\mathrm{h}}41^{\mathrm{m}}$, $\delta = 05°03'$. One should notice that some stars appear stretched due to proximity to frame edge and off-axis optical effect. The satellite was identified by correlation with expected position.

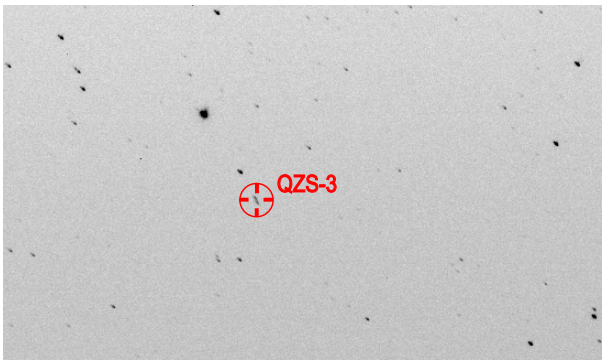


Figure 8: Satellite QZS-3 (NORAD ID: 42917), source: POLON-Australia_B, epoch (UTC): 2024-06-17T12:29:33.134

In Fig. 9, the OD fitting residuals using batch least squares (BLS) optimization performed using two computational engines, namely Orbit Determination Toolbox (ODTK) and Orekit, and the data collected for the QZS-3 (Table 5) in the course of the experiment (Fig. 7), have been presented. For both ODTK (Fig. 9a) and Orekit (Fig. 9b), an analogous distribution of residues as well as roughly similar accuracy of orbit fitting was achieved.

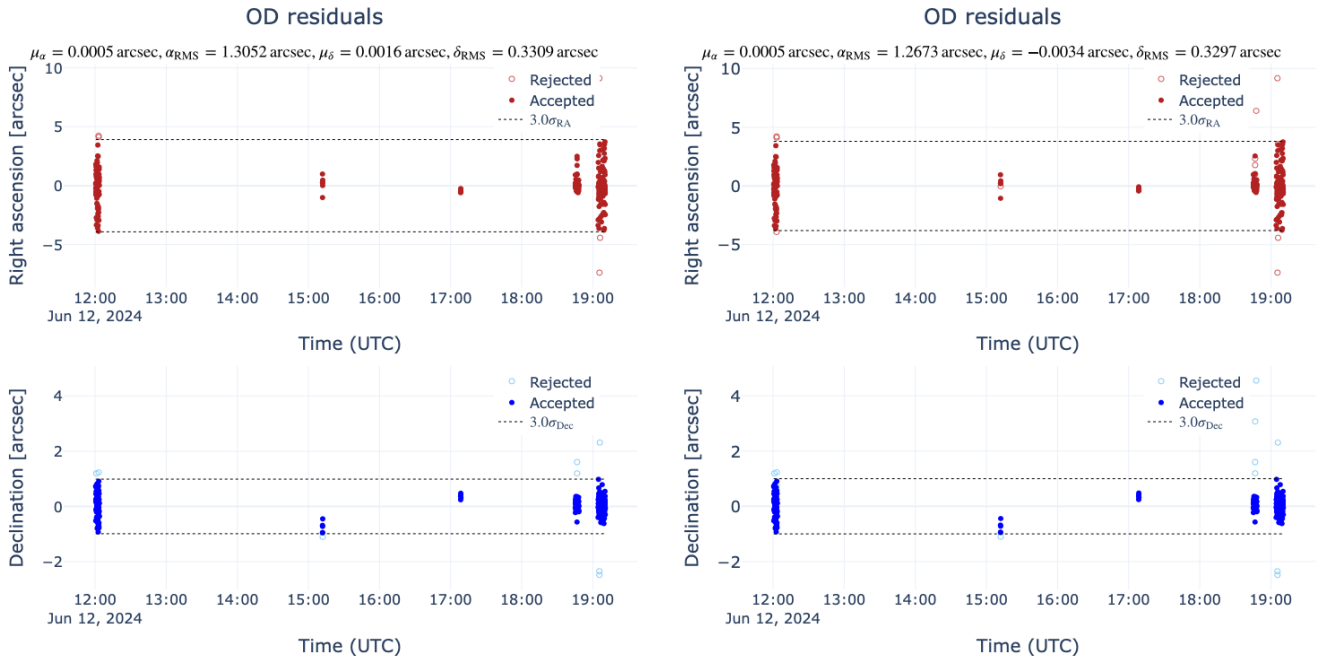


(a) ODTK-based results

(b) Orekit-based result

Figure 9: QZS-3 (NORAD ID: 42917) BLS-based OD results

### 5.2.2 Experiment 2: GEO tracking

**POLON operational conditions** Analogously as in case of GEO-S, the GEO-T campaigns' total duration reached 8 d 18 h. During this period, given the observational conditions and the operational status of the assets, the observational opportunities available at each location have been illustrated in Fig. 10. Site POLON-Australia was accessible for about 2 days 6 hours (31.3% of the possible time), POLON-Chile for 6 days 12 hour (87.6%), and POLON-Africa was not available during this period due to weather constraints.

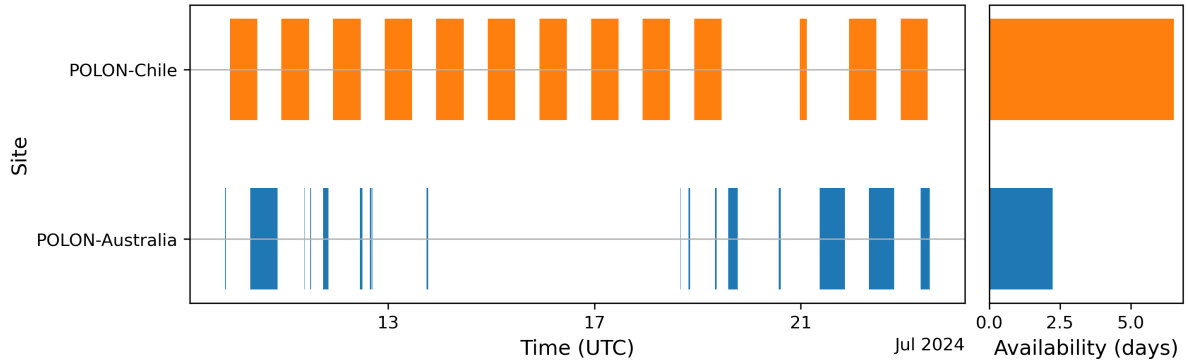


Figure 10: Availability of sensors for observations per site during GEO tracking experiment

**POLON performance** POLON performance metrics for GEO tracking experiment are summarized in table 6. As with the GEO survey experiment, those metrics indicate a high overall throughput of POLON sensors. Given the maximum observable arc length of 3.75° for a sensor with a fixed 15-minute timeslot, the arc lengths measured are satisfactory and in some cases even close to the maximum. Regarding the number of unique objects observed, we focused on tracking as many objects as possible, what can also be clearly seen in the revisit histogram in fig. 11. 617 objects have been observed out of 1206 possible.

Table 6: GEO-T campaign performance statistics

| Metric ($\boldsymbol{J}_{\mathrm{M}}$) | Unit/Format | Value | | | | | |
|---|---|---|---|---|---|---|---|
| | | min | max | median | mean | std | total |
| Astrometric RMS ($J_{\mathrm{MARMS}}$) | arcsec | 0.13 | 1.39 | 0.30 | 0.28 | N/A | N/A |
| Arc Length ($J_{\mathrm{MLARC}}$) | deg | 0.01 | 3.73 | 1.21 | 1.24 | N/A | N/A |
| No. of measurements ($J_{\mathrm{MMEAS}}$)** | | 3 | 269 | 32 | 48 | 48 | 302562 |
| Objects observed ($J_{\mathrm{MSO}}$)* | | | | | | | 6200 |
| Unique objects ($J_{\mathrm{MUSO}}$) | | | | | | | 617 |

* No. of objects observed is equivalent to number of TDMs generated ($\Omega_{\mathrm{M}}$) — recall Section 4: Data acquisition, storage and processing.
** The statistics are given per TDM.

Revisit histogram is presented in Fig. 11. As in case of GEO-S, the results presented indicate that POLON was used effectively during the campaign, where most of the objects were observed once during the course of the experiment, with some being observed twice or thrice.

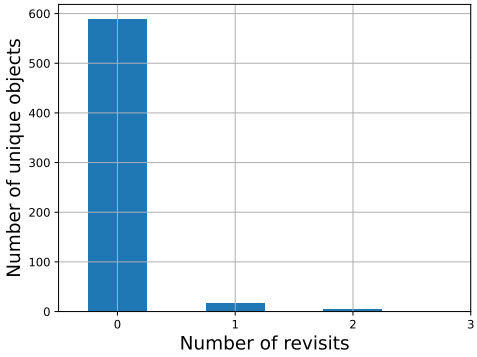


Figure 11: POLON unique objects revisits during GEO-T campaign

### 5.2.3 Experiment 3: LEO tracking

**POLON operational conditions** In case of LEO-T campaign its total duration reached 2 d 3 h. During this period, given the observational conditions and the operational status of the assets, the observational opportunities available at each location have been illustrated in Fig. 12. Site POLON-Australia was accessible for about 16 hours (62.6% of the possible time), POLON-Chile for 1 day 7 hours (96.6%), and POLON-Africa for 4 hours (13.9%).

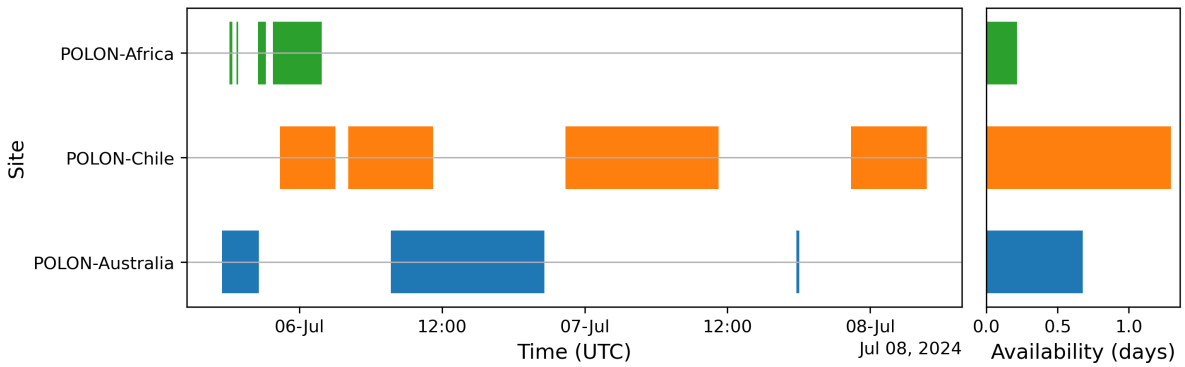


Figure 12: Availability of sensors for observations per site during LEO experiment

**POLON performance** Due to aforementioned short duration of the LEO tracking experiment, it is hard to draw reliable conclusion from the metrics presented in table 7. A significant variability in arc lengths observed should be noticed. Sparse, weather-constrained, availability of POLON-Africa and POLON-Australia seen in Fig. 12 biases the statistics presented. On the other hand, out of 40 tasked objects, 30 have been observed, giving a 75% efficiency.

Table 7: Campaign no. 1 performance statistics

| Metric ($\boldsymbol{J}_{\mathrm{M}}$) | Unit/Format | Value | | | | | |
|---|---|---|---|---|---|---|---|
| | | min | max | median | mean | std | total |
| Astrometric RMS ($J_{\mathrm{MARMS}}$) | arcsec | 0.10 | 0.52 | 0.18 | 0.18 | N/A | N/A |
| Arc Length ($J_{\mathrm{MLARC}}$) | deg | 0.08 | 141.45 | 6.64 | 10.71 | N/A | N/A |
| No. of measurements ($J_{\mathrm{MMEAS}}$)** | | 3 | 662 | 37 | 65 | 80 | 28488 |
| Objects observed ($J_{\mathrm{MSO}}$)* | | | | | | | 435 |
| Unique objects ($J_{\mathrm{MUSO}}$) | | | | | | | 30 |
| Tasked objects | | | | | | | 40 |

* No. of objects observed is equivalent to number of TDMs generated ($\Omega_{\mathrm{M}}$) — recall Section 4: Data acquisition, storage and processing.
** The statistics are given per TDM.

Revisit histogram is presented in Fig. 13. As can be clearly seen, emphasis was placed on maximizing the amount of unique objects observed, however a significant portion of objects were revisited at least once.

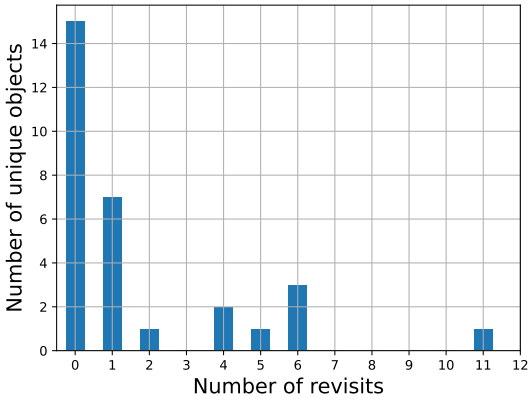


Figure 13: POLON unique objects revisits during LEO-T campaign

**OD based assessment** The orbital accuracy of the observations acquired during the LEO-T campaign was assessed using the observation of both LEO objects and complimentary MEO satellites. These include two case studies. First, the LAGEOS 1 (NORAD ID: 8820). Second, the EGS (AJISAI) (NORAD ID: 16908). Objects details have been provided in Table 8.

Table 8: LAGEOS 1 and EGS (AJISAI) satellite object characterization

| Parameter | Unit/Format | Value | | Source/Description |
|---|---|---|---|---|
| | | Case 1 | Case 2 | |
| Object name | N/A | LAGEOS 1 | EGS (AJISAI) | space-track.org |
| NORAD ID | N/A | 8820 | 16908 | space-track.org |
| COSPAR ID | N/A | 1976-039A | 1986-061A | celestrak.org |
| Type | N/A | Payload | Payload | space-track.org |
| Avg. cross-section | $m^2$ | 0.2827 | 3.631 | celestrak.org |
| Mass | kg | 411.0 | 678.89 | celestrak.org |
| Launch date | UTC | May 4, 1976 | Aug 12, 1986 | space-track.org |

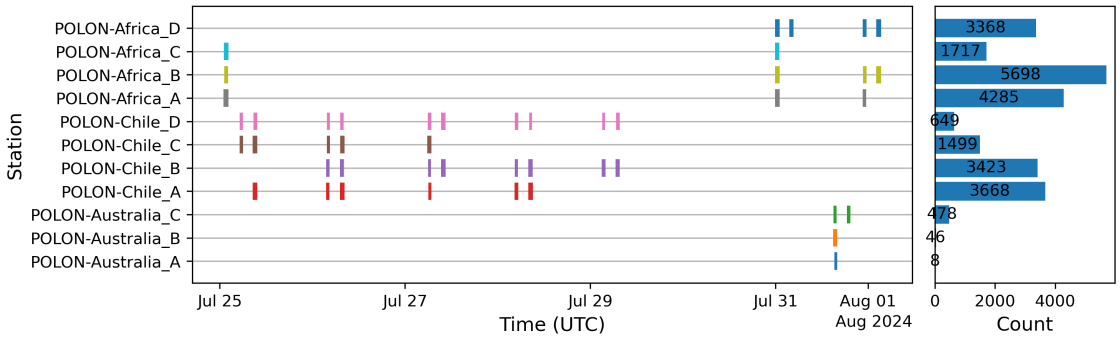


(a) LAGEOS 1 (NORAD ID: 8820)

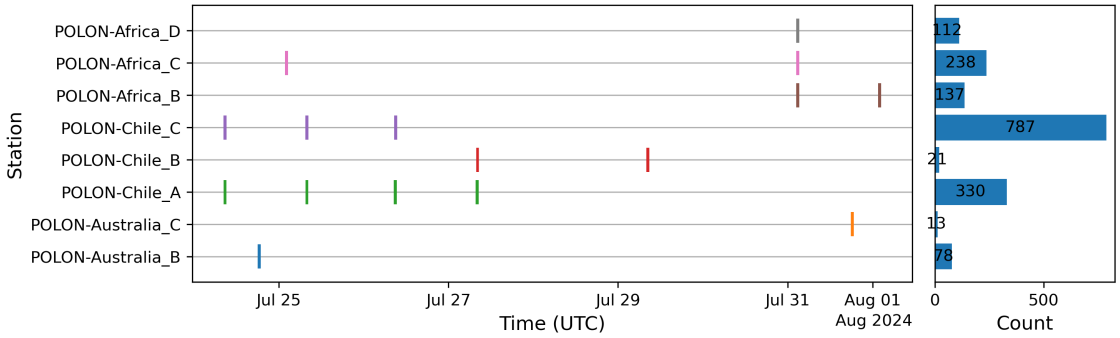


(b) EGS (AJISAI) (NORAD ID: 16908)

Figure 14: Observation events during LEO-T case studies

In Fig. 15 two cutouts from photos in FITS format, taken during the LEO experiment, have been presented. The first one was captured using exposure time of $0.5\,s$ and binning $2 \times 2$, with POLON-Africa_D telescope on 19.06.2024 at $02:59:20$ UTC (mid-exposure) and shows the position of LAGEOS 1 satellite. The original frame center coordinates yields: $\alpha = 19^{\mathrm{h}}26^{\mathrm{m}}$, $\delta = -57^{\circ}17'$. The second one was captures with the exposure time of $0.4\,s$ and binning $2 \times 2$, with POLON-Africa_B telescope on 02.08.2024 at $03:02:15$ UTC (mid-exposure) and presents the position of EGS (AJISAI) satellite. The original frame center coordinates yields: $\alpha = 10^{\mathrm{h}}26^{\mathrm{m}}$, $\delta = -84^{\circ}24'$.

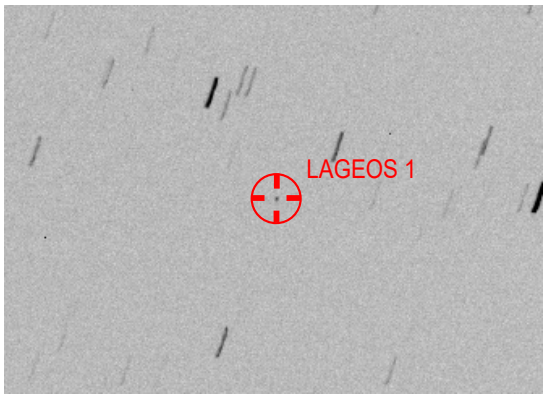


(a) LAGEOS 1 (NORAD ID 8820), source: POLON-Africa_D, epoch (UTC): 2024-08-19T02:59:20.567

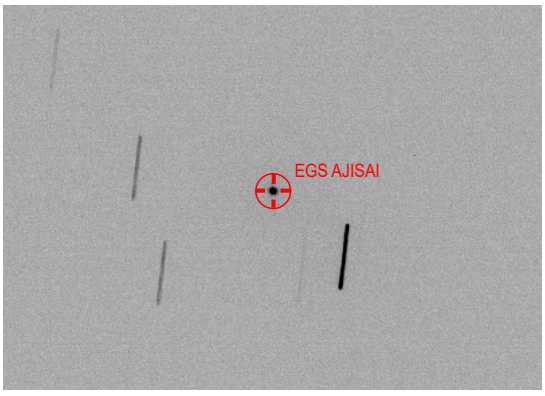


(b) EGS (AJISAI) (NORAD ID 16908), source: POLON-Africa_B, epoch (UTC): 2024-08-02T03:02:15.322

Figure 15: Observation events during LEO-T case studies

In Fig. 16, the OD residuals using BLS optimization performed using ODTK analytical engine and the data collected for the LAGEOS 1 and EGS AJISAI objects (Table 8) in the course of the experiment (Fig. 14), have been presented.

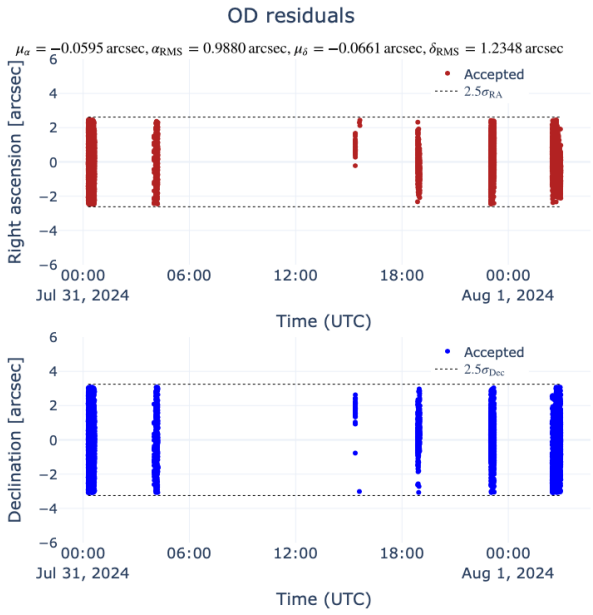


(a) ODTK-based results

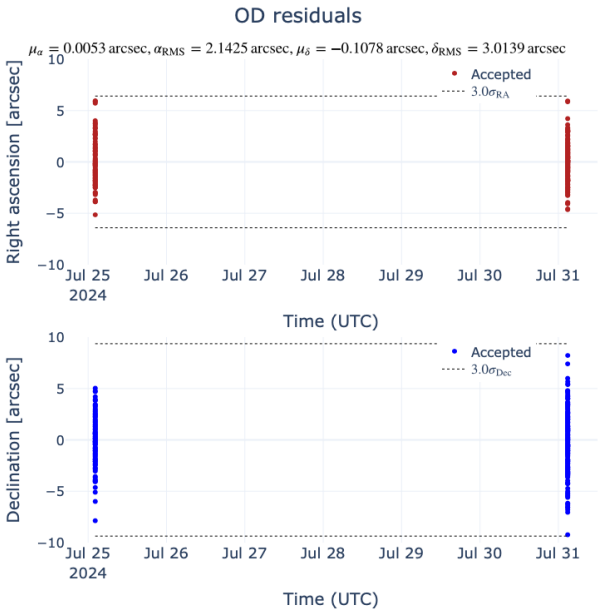


(b) ODTK-based results

Figure 16: LAGEOS 1 (NORAD ID: 8820) and EGS (AJISAI) (NORAD ID: 16908) BLS-based OD results

In addition, Fig. 17 illustrates the OD results obtained for LAGEOS (NORAD ID: 8820) and EGS (AJISAI) (NORAD ID 16908) objects (Table 8) using an alternative method, namely the Unscented Kalman Filter (UKF), implemented in ODTK. Comparing the distribution of residuals it is noticeable that both algorithms (Fig. 17 and Fig. 16) allow for successful OD. Although, the practical use of both and the interpretation of residuals is slightly different.

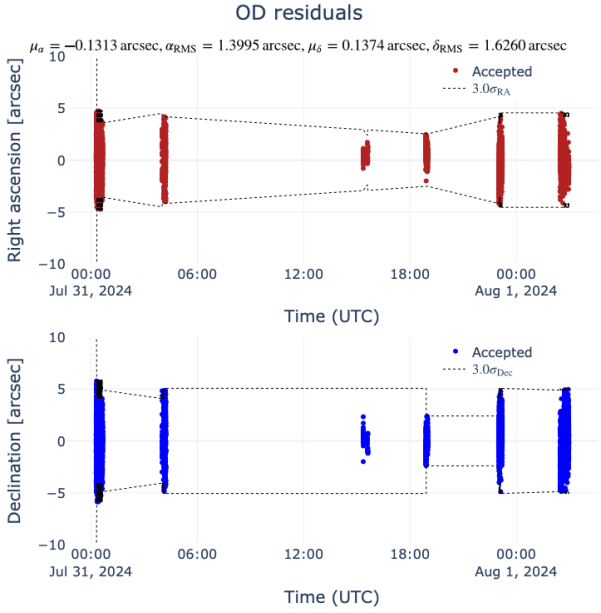


(a) LAGEOS 1 (NORAD ID: 8820) ODTK-based results

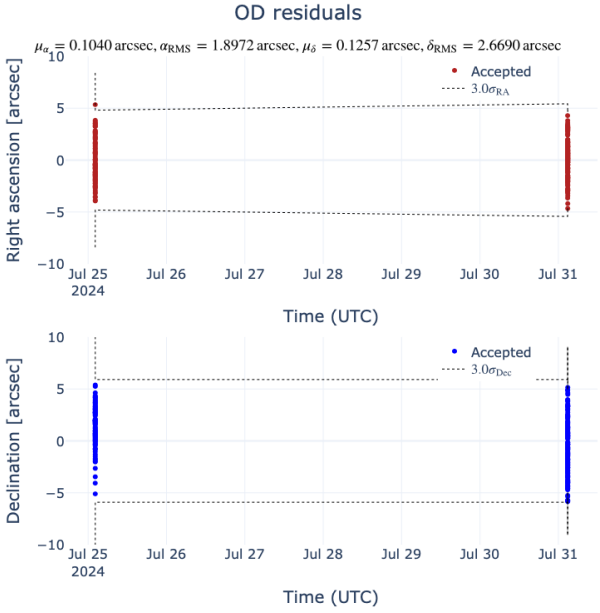


(b) EGS (AJISAI) (NORAD ID: 16908) ODTK-based results

Figure 17: LAGEOS 1 (NORAD ID: 8820) and EGS (AJISAI) (NORAD ID: 16908) UKF-based OD results

### 5.2.4 Operational use-cases

Several selected operational use-cases (UCs) of POLON and data from this network are presented in this section. These include: *UC-1:* RESURS-P1 (NORAD ID: 39186) fragmentation event observations, *UC-2:* CZ-3B R/B (NORAD ID: 58254) re-entry event prediction using POLON data-based OD results, *UC-3:* ESA Jupiter Icy Moon Explorer (JUICE) dual gravity assist.

**UC-1: RESURS-P1 (39186) fragmentation event** POLON network is well-suited for monitoring fragmentation events. Large FoV combined with the presence of 4 telescopes per site allows the tracking of multiple fragments even if visible passes are infrequent. RESURS-P1 was a Russian Earth Observation Satellite launched on 25.06.2013. It sufferred a fragmentation event on 26.06.2024, and we decided to observe the fragments.

In Fig. 18, cutouts from photos in FITS format, showing the positions of some RESURS P1 fragments, are presented. All shown photos have been captured using exposure time of $0.5\,s$ and binning $2 \times 2$. Midexposure times and original frame centers coordinates are: Fig. 18a captured on 07.07.2024 at $04:34:00$ UTC on coordinates $\alpha = 21^{\mathrm{h}}37^{\mathrm{m}}$, $\delta = 72°44'$; Fig. 18b captured on 07.07.2024 at $04:33:06$ on coordinates $\alpha = 11^{\mathrm{h}}05^{\mathrm{m}}$, $\delta = 24°15'$; Fig. 18c captured on 07.07.2024 at $04:36:16$ on coordinates $\alpha = 16^{\mathrm{h}}00^{\mathrm{m}}$, $\delta = -21°57'$; Fig. 18d captured on 07.07.2024 at $04:36:33$ on coordinates $\alpha = 20^{\mathrm{h}}53^{\mathrm{m}}$, $\delta = 11°57'$. This demonstrates that POLON is capable of providing a support to fragmentation events with observations of nearly simultaneous flybys of fragments in different parts of the sky.

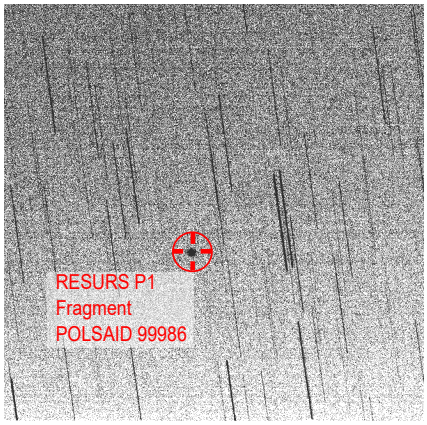


(a) Source: POLON-Utah_C, epoch (UTC): 2024-07-07T04:33:59.766

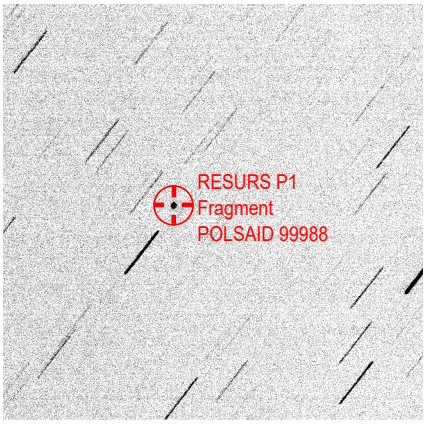


(b) Source: POLON-Utah_B, epoch (UTC): 2024-07-07T04:33:06.708

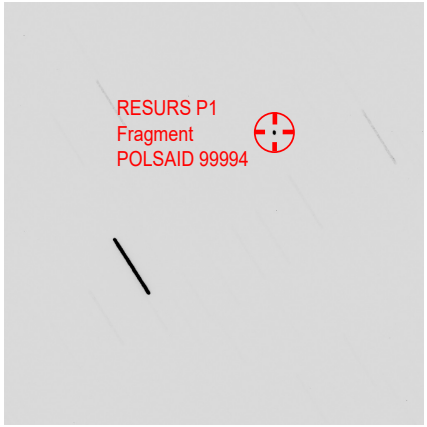


(c) Source: POLON-Utah_B, epoch (UTC): 2024-07-07T04:36:16.243

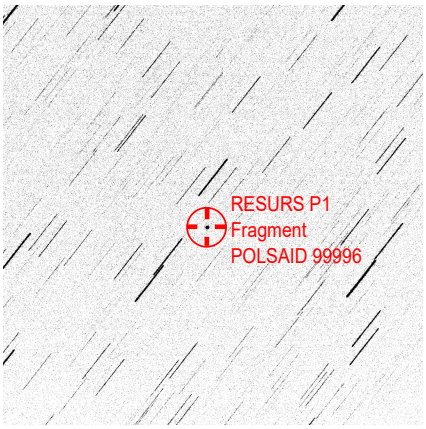


(d) Source: POLON-Utah_C, epoch (UTC): 2024-07-07T04:36:33.103

Figure 18: RESURS P1 debris detection, FITS cutouts. 4 fragments, POLSA ID 99986, 99988, 99994 & 99996, have been observed, with 275, 293, 50 and 170 measurements respectively.

**UC-2: CZ-3B R/B (NORAD ID: 58254) Re-entry event** Passive optical telescopes can be used to support prediction of the re-entry (RE) moment of satellite objects. Since POLON telescopes are able to observe low-altitude objects, and based on these observations it is possible to refine orbital parameters and better predict the RE moment [17].

Let the object of interest be characterized as in Table 9.

Table 9: CZ-3B R/B satellite object characterization

| Parameter | Unit/Format | Value | Source/Description |
|---|---|---|---|
| Object name | N/A | CZ-3B R/B | space-track.org |
| NORAD ID | N/A | 58254 | space-track.org |
| COSPAR ID | N/A | 2023-172B | celestrak.org |
| Type | N/A | Rocket body | space-track.org |
| Avg. cross-section | $m^2$ | 32.704 | discosweb.esoc.esa.int |
| Mass | kg | 2740.0 | discosweb.esoc.esa.int |
| Launch date | UTC | Nov 9, 2023 | space-track.org |

Based on the observations from telescopes POLON-Chile (3 tracks, acquired 9.04.2024) it was possible to determine orbit and predict RE epoch. The formal uncertainty of the obtained solution is defined as 20% of the time to RE (Fig. 19), while the actual difference between the predicted RE epoch and the actual one is not greater than 8% (Fig. 20), which indicates a good precision of the observations and an adequate method of predicting the RE moment.

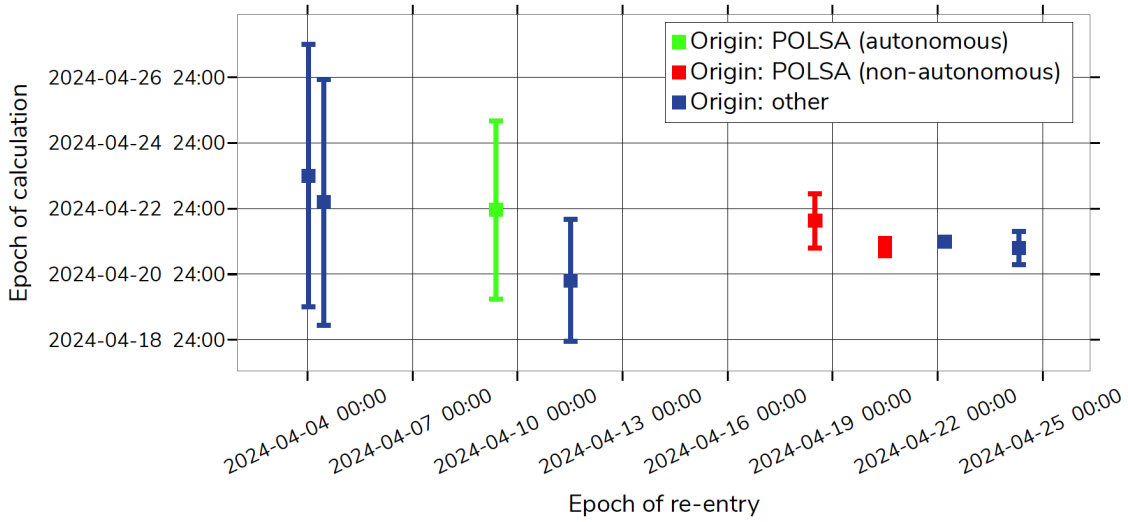


Figure 19: Estimated Re-entry Window Evolution

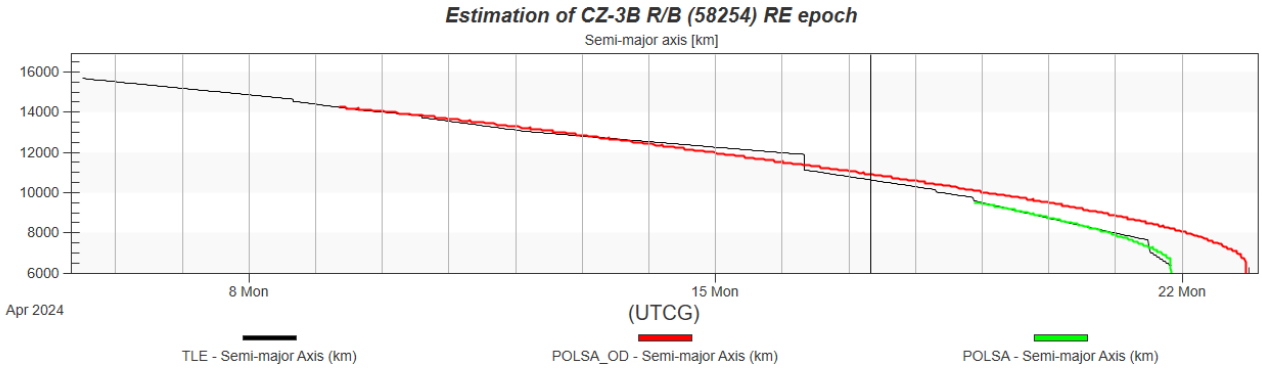


Figure 20: Semi-major axis of CZ-3B R/B (NORAD ID: 58254)

**UC-3: JUICE dual gravity assist** JUICE is a deep space mission by European Space Agency (ESA), with primary goal of exploring Jupiters' moons Europa, Ganymede and Callisto. The probe was launched on 14th April 2023. To conserve propellant, multiple gravity assists are used instead of direct Hohmann transfer. First such assist was a flyby of Earth and Moon occurring on 19-20.08.2024. After the event, the POLON network was tasked to observe JUICE in the next stage of the mission. Unfortunately, observations prior to the closest approach were not feasible considering a very small angular distance from the spacecraft to the Moon; violating the telescope's safety constraints. Instead, observations were carried out shortly after the closest approach.

The observation task was prepared using the coordinates from NASA's Horizons system [20]. For this purpose, the sensor was configured for observations in survey mode, with star tracking. Since there was considerable uncertainty regarding the expected brightness of the observed object, observations were conducted with a wide range of exposure times. The observations with exposure times ranging from 10 s to 30 s resulted in a weak but clear detection.

In Fig. 21 the results obtained in the form of FITS cutouts have been depicted, with the position of the spacecraft marked. Frames illustrated in Fig. 21a have been captured on 21.08.2024 between 08 : 46 : 05 UTC and 09 : 13 : 16 UTC with exposure time of 10 $s$, binning of $2 \times 2$, and original frame center coordinates $\alpha = 15^{\mathrm{h}}03^{\mathrm{m}}$, $\delta = -14^{\circ}45'$; Fig. 21b depicts photos taken on 21.08.2024 between 23 : 15 : 44 UTC and 23 : 39 : 59 UTC with exposure time of 15 $s$, binning of $2 \times 2$, and original frame center coordinates $\alpha = 15^{\mathrm{h}}25^{\mathrm{m}}$, $\delta = -16^{\circ}43'$.

To verify that the detected object is indeed the JUICE spacecraft, astrometry was performed, and celestial position as well as tangential angular speed and its direction were compared with results provided by NASA Horizons. All parameters matched well, which provides a high confidence of positive detection.

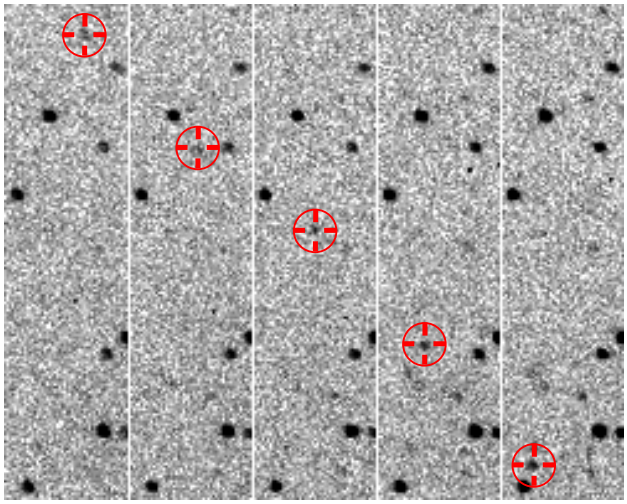

(a) Average time between frames is about 6 minutes 45 seconds, first photo is on the left. Source: POLON-Australia_B, epoch (first slice, UTC): 2024-08-21T08:46:05.248

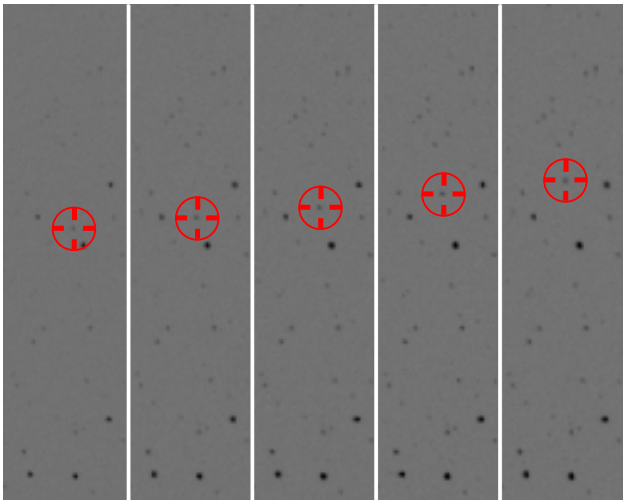

(b) Average time between displayed frames is about 6 minutes, first photo is on the left. Source: POLON-Chile_C, epoch (first slice, UTC): 2024-08-21T23:15:44.002

Figure 21: JUICE probe flyby. Each photo presents 5 FITS file cutouts taken during the observation period.

## 6. CONCLUSIONS

In this experimental work, the authors focused on the problem of comparing POLON performance and observational efficiency using well-defined indices in survey and tracking modes. The astrometric and orbital performance of the POLON-based data has been demonstrated. Moreover, a feasibility study of survey and tracking scheduling of POLON and system-level responses for the GEO, MEO, and LEO regimes has been documented, based on conducted experiments and operational use-cases. Main findings include the following. First, the main advantage of POLON is its global distribution. This not only provides access to a wide population of objects, but also makes it possible to track a selected object from different locations, which improves the orbit determination process. The second important feature of the system is the configuration of a single sensor location itself. The use of a sensor mesh (multiple configurations) not only provides a very large field of view for survey observations, but also provides the capability to track multiple objects at once. Both of these aspects were demonstrated experimentally through the observation campaigns carried out. At the same time, the results obtained indicate that despite the use of four

configurations at each location, the number of configurations could still be larger given the large population of space objects. Thus, the development of POLON in the future can be considered as justified. A third important feature to note is the simplicity with which POLON enables routine observations of objects in orbits spanning from GEO to LEO. At the same time, it is worth noting that POLON's technical capabilities are far more extensive. This is documented on the example of operational use-cases. These capabilities extend to objects approaching re-entry and those at a considerable distance from Earth — JUICE.

## ACKNOWLEDGMENTS

The authors acknowledge the Ministry of Economic Development and Technology Republic of Poland, European Commission, Directorate-General Defence Industry and Space, and the European Health and Digital Executive Agency's organizational and financial support under grant 2-3SST2018-20, Specific agreement no. 952852, Decision no. 541/2014/EU, due to which the POLON can foster European Cooperation in the SST domain as a part of national and European endeavors.

### CRediT authorship contribution statement

**Tomasz Zubowicz** Project administration, Supervision, Conceptualization, Methodology, Investigation, Formal analysis, Software, Validation, Visualization, Writing - Original Draft, Writing - Review & Editing; **Mikołaj Krużyński** Supervision, Conceptualization, Methodology, Investigation, Formal analysis, Visualization, Writing - Original Draft, Writing - Review & Editing; **Krzysztof Armiński** Conceptualization, Methodology, Investigation, Formal analysis, Investigation, Visualization, Writing - Original Draft, Writing - Review & Editing; **Krzysztof Szyszka** Resources, Data Curation, Investigation, Formal analysis, Visualization, Writing - Original Draft; **Marcin Teofilewicz** Resources, Data Curation, Investigation, Formal analysis, Writing - Original Draft; **Mikołaj Karawacki** Resources, Data Curation, Investigation, Formal analysis, Visualization, Writing - Original Draft; **Artur Makarewicz** Resources; **Edwin Wnuk** Supervision, Conceptualization, Methodology, Writing - Original Draft, Writing – review & editing; **Zygmunt Anioł**[3] Resources, Writing - Original Draft, Writing – review & editing ; **Tymoteusz Trocki**[4] Conceptualization.

## REFERENCES

[1] Bruno Coelho, Domingos Barbosa, Miguel Bergano, João Pandeirada, Paulo Marques, Alexandre Correia, and José Matias de Freitas. Developing a data fusion concept for radar and optical ground based sst station. *arXiv preprint arXiv:2211.04443*, 2022.

[2] D.A. Vallado and W.D. McClain. *Fundamentals of Astrodynamics and Applications*. Fundamentals of Astrodynamics and Applications. Microcosm Press, 2001.

[3] H. Hurnik, R. Baranowski, W. Naskrecki, B. Furmann, and S. Łoś. A mobile satellite laser ranging system of 2-nd generation. *Artificial Satellites*, 26(1):19–30, Jan 1991.

[4] Stanisław Schillak, Paweł Lejba, Piotr Michałek, Tomasz Suchodolski, Adrian Smagło, and Stanisław Zapaśnik. Analysis of the Results of the Borowiec SLR Station (7811) for the Period 1993–2019 as an Example of the Quality Assessment of Satellite Laser Ranging Stations. *Sensors*, 22(2):616, January 2022.

[5] K. Kaminski, E. Wnuk, J. Golebiewska, M. Kruzynski, P. Kankiewicz, and M. Kaminska. High efficiency robotic optical tracking of space debris from PST2 telescope in Arizona. In *7th European Conference on Space Debris*, page 188, Apr 2017.

[6] Global astrophysical telescope system homepage. https://www.astro.amu.edu.pl/~chrisk/gats/index.php. Accessed on August 25th, 2024.

[7] Krzysztof Kamiński, Michał Żołnowski, Edwin Wnuk, Justyna Gołębiewska, Mikołaj Krużyński, Monika K. Kamińska, and Marcin Gędek. Low LEO optical tracking observations with small telescopes. In *1st NEO and Debris Detection Conference_ESA2019*, page 27, Jan 2019.

[8] S. K. Kozłowski, P. W. Sybilski, M. Konacki, R. K. Pawłaszek, M. Ratajczak, K. G. Hełminiak, and M. Litwicki. Project Solaris, a Global Network of Autonomous Observatories: Design, Commissioning, and First Science Results. *PASP*, 129(980):105001, Oct 2017.

[9] 6ROADS homepage. https://www.6roads.com.pl. Accessed on August 25th, 2024.

[3]POLON Project Executive Officer under 2-3SST2018-20 grant

[4]POLON Project Management Officer under 2-3SST2018-20 grant

[10] Krzysztof Kaminski, Edwin Wnuk, Justyna Golebiewska, Mikolaj Kruzynski, Monika K. Kaminska, Michal Zolnowski, Marcin Gedek, and Jacek Pala. New Optical Sensors Cluster for Efficient Space Surveillance and Tracking. In S. Ryan, editor, *The Advanced Maui Optical and Space Surveillance Technologies Conference*, page 48, Sep 2018.

[11] EU SST Partnership. https://www.eusst.eu. Accessed on August 28th, 2024.

[12] Simon Haykin and K. J. Ray Liu. *Handbook on Array Processing and Sensor Networks*. John Wiley & Sons, Ltd, 2010.

[13] Hairong Qi, S.Sitharama Iyengar, and Krishnendu Chakrabarty. Distributed sensor networks—a review of recent research. *Journal of the Franklin Institute*, 338(6):655–668, 2001. Distributed Sensor Networks for Real-time Systems with Adaptive C onfiguration.

[14] Igone Urdampilleta, Emmanuel Delande, Vincent Morand, Johannes Gelhaus, Elena Vellutini, Violeta Poenaru, José Freitas, Tomasz Zubowicz, and Daniel Garcia-Yarnoz. System Approach to Analyse the Performance of the current and future EU Space Surveillance and Tracking system at Service Provision level. In *22th AMOS conference proceedings*. Maui Economic Development Board, September 2022.

[15] Krzysztof Armiński, Tomasz Zubowicz, Stefania Wolf, Mikołaj Krużyński, Zygmunt Anioł, Tymoteusz Trocki, and Edwin Wnuk. A multi-objective approach to the optimal selection of assets for the design of an optical sensor network. In *24th AMOS conference proceedings*. Polish Space Agency (POLSA), Maui Economic Development Board, September 2023.

[16] J. Agre and L. Clare. An integrated architecture for cooperative sensing networks. *Computer*, 33(5):106–108, 2000.

[17] Mikołaj Krużyński, Zygmunt Anioł, Krzysztof Armiński, Dorota Mieczkowska, Marcin Teofilewicz, Edwin Wnuk, and Tomasz Zubowicz. Influence of the atmosphere model and the quality of the ballistic coefficient (bc) estimation on the prediction of the re-entry moment. In *24th AMOS conference proceedings*. Polish Space Agency (POLSA), Maui Economic Development Board, September 2023.

[18] R. E. Kalman and R. S. Bucy. New Results in Linear Filtering and Prediction Theory. *Journal of Basic Engineering*, 83(1):95–108, 03 1961.

[19] Agnieszka Sybilska, Stanisław Kozłowski, Piotr Sybilski, Rafal Pawłaszek, Mariusz Słonina, Agnieszka Gurgul, Piotr Konorski, Michał Drzał, Sławomir Hus, Grzegorz Lech, Michał Litwicki, Maciej Pilichowski, Rafał Ślimak, Ulrich Kolb, Vadim Burwitz, Tim Flohrer, and Quirin Funke. Astrometry24.net – precise astrometry for SST and NEO. In *1st NEO and Debris Detection Conference_ESA2019*, page 10, Jan 2019.

[20] JPL Horizons on-line solar system data and ephemeris computation service. https://ssd.jpl.nasa.gov/horizons/app.html#/. Accessed on August 28th, 2024.